ACS APPLIED MATERIALS & INTERFACES

Research Article

www.acsami.org

Deformation of Confined Poly(ethylene oxide) in Multilayer Films

Chuan-Yar Lai, Anne Hiltner,† Eric Baer, and LaShanda T.J. Korley*

Department of Macromolecular Science and Engineering, and the Center for Layered Polymeric Systems, Case Western Reserve University, Cleveland, Ohio 44106-7202, United States

Supporting Information

ABSTRACT: The effect of confinement on the deformation behavior of poly(ethylene oxide) (PEO) was studied using melt processed coextruded poly(ethylene-co-acrylic acid) (EAA) and PEO multilayer films with varying PEO layer thicknesses from 3600 to 25 nm. The deformation mechanism was found to shift as layer thickness was decreased between 510 and 125 nm, from typical axial alignment of the crystalline fraction, as seen in bulk materials, to nonuniform micronecking mechanisms found in solution-grown single crystals. This change was evaluated via tensile testing, wide-angle X-ray diffraction (WAXD), atomic force microscopy (AFM), and differential scanning calorimetry (DSC). With the commercially relevant method of melt coextrusion, we were able to overcome the limitations to the testing of solution-grown single crystals, and the artifacts that occur from their handling, and bridged the gap in knowledge between thick bulk materials and thin single crystals.

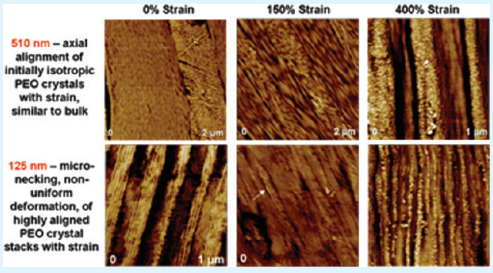

KEYWORDS: *single crystal, deformation, polyethylene oxide*

INTRODUCTION

There has been much interest in the mechanism of plastic deformation of semicrystalline polymers since the 1960s, when polymers were emerging as commercial products. As these types of polymers are useful for many applications, their mechanical properties are of great importance. Several studies have examined bulk materials, single crystals, and single crystal mats of polyethylene (PE), polypropylene (PP), polyesters, and polyoxymethylene (POM), with very distinct structures resulting from deformation due to the large differences in scale and crystalline orientation.[1−14] However, there has been little investigation of the deformation of semicrystalline polymers as a function of thickness spanning the thicknesses between bulk and single crystals, as it was difficult to obtain samples of various thicknesses using a single process.

A vast amount of literature on the deformation of bulk polymers exists today. It has been widely accepted that the process of deformation for bulk materials with a spherulitic morphology progresses in the following manner: (1) interlamellar deformation of the amorphous phase and elongation of amorphous tie chains, (2) shearing and tilting of lamellar chain folds where twinning and phase transformations can also occur, (3) separation of the crystalline block segments, and (4) orientation of the block segments and tie chains and/or chain pullout and recrystallization.[1−8] Crystal alignment in relation to the deformation axis greatly affects the amount of interlamellar deformation and the onset time of subsequent steps. The most interlamellar deformation and voiding are observed when the crystalline lamellae are aligned perpendicular to the deformation direction, which delays crystal shearing and tilting, and the least amount observed when the lamellae are aligned parallel to the direction of deformation.

The abundance of studies on polymeric single crystal deformation has been focused on small amounts of solution-grown samples of single crystals or single crystal mats. These single crystals were deposited on substrates, such as Mylar, which limited the studies to strains below 200%.[9−14] After stretching, carbon replicas of the crystals were produced through a shadowing process, and these were imaged using electron diffraction and scanning electron microscopy (SEM). Cracks and nonuniform deformation, called micronecking, were observed. The deformation mechanism was found to be dependent upon which crystal axis was aligned with the deformation direction in PE,[11−13] POM,[9,10,13] and polyesters.[14] Cracks and minimal deformation were observed along one axis, while micronecking, as well as uniform deformation, were observed along the other axis. Artifacts were often detected due to crystal slip from the substrate and to greater relaxation of the substrate than the crystal, and as a result of the replication process. Though these were important findings, the limitations to the testing of solution-grown single crystals, and the artifacts that occur from their handling, make it difficult to compare with present commercial polymers. It would be beneficial to examine these types of structures under conditions more relevant to the current processing and testing methods of semicrystalline polymers, which often involve melt processing and larger sample volumes.

Rigidly confined thin films without a free surface can be fabricated by microlayer coextrusion with layer thicknesses from multiple micrometers down to nanometers.[15,16] As the thickness of a confined PEO layer decreases from the

Received: February 10, 2012
Accepted: April 5, 2012
Published: April 16, 2012

microscale to the nanoscale, the morphology systematically changes from three-dimensional spherulites to two-dimensional discoids and to 'in-plane' lamellar stacks.[17] Finally, when the confinement occurs on the 25 nm size scale of the usual lamellar thickness, the PEO layers crystallize as single lamellae with a large aspect ratio that resemble large single crystals.[18] A previous study on low strain deformation of confined PEO yielded unexpected results due to the high orientation of PEO as layer thickness decreased.[19] In this work, we advance our understanding, highlighting the shift in deformation mechanism as a result of PEO layer thickness. PEO was coextruded as microlayer and nanolayer films with up to 1025 layers of PEO alternating with poly(ethylene-*co*-acrylic acid) (EAA). The number of layers and composition was adjusted to achieve individual layer thicknesses ranging from a few micrometers to 20 nm. Using these multilayer films, conventional experimental methods can be used to study the effect of thickness on the deformation of PEO, with the ability to stretch the PEO to high strains and image the resulting structures, which have been previously unachievable.

EXPERIMENTAL SECTION

The confined polymer of high crystallinity, ~70%, used in this study is poly(ethylene oxide) (PEO) (Polyox WSR-N80), with a molecular weight of ~200 000 g/mol, and melting point of 65 °C. The alternate layer that confines PEO is an ethylene-co-acrylic acid copolymer (EAA), Primacor 1410, with a melting temperature at 99 °C. All materials were obtained from Dow Chemical. The materials characteristics, melting temperature (T_m) and crystallinity (X_c), are summarized in Table 1.

Table 1. Polymer Material Characteristics

	material	grade	T_m (°C)	X_c (wt %)
confining material	ethylene-*co*-acrylic acid (EAA) (AA 9.7 wt %)	Primacor 1410	99	31
confined material	poly(ethylene oxide) (PEO)	WSR-N80	65	73

For this study, films with 33, 257, and 1025 alternating EAA and PEO layers with EAA/PEO 50/50 (vol./vol.) composition and 1025-layer EAA/PEO 90/10 composition were produced through a continuous coextrusion process.[20,21] Change in the number of layers and composition allowed for a large range of layer thicknesses. The overall film thicknesses ranged from 120 to 130 μm, which corresponded to individual PEO layer thicknesses of 25–3600 nm. Table 2 summarizes the characteristics of these layered samples. Films were dried and kept stored in a desiccator with molecular sieves before all testing.

The stress–strain behavior in uniaxial tension was measured according to ASTM D1708[22] with microtensile specimens cut from each extruded film along the extrusion direction. Three specimens of each film were stretched in an MTS (Eden Prairie, MN) Alliance RT30 at a strain-rate of 100% min^{-1} at T = 23 °C. Engineering stress and strain were defined conventionally. Tensile modulus values were taken at 1% strain. Samples for 2D WAXD were prepared by stretching 8 mm long, 2 mm wide strips to various strains: 50, 100, 150, and 250. Larger 8 mm long, 4 mm wide strips were used to obtain samples stretched to 400%. While being held in tension, the strips were clamped down in a metal holder before release from the MTS grips, preserving an 11 mm long strip of unrecovered sample. Though data was collected at 0%, 50%, 100%, 150%, 250%, and 400% strain, we will only show raw data for 0%, 150%, and 400%.

Wide-angle X-ray scattering (WAXS) measurements were carried out using a Micromax002+ X-ray generator (Rigaku, Woodlands, TX), operated at 45 kV and 0.88 mA, producing a highly focused parallel beam of monochromatic Cu K_α radiation (λ = 0.154 nm). Transverse direction (TD) 2D patterns were collected by aligning the incident X-ray beam parallel to the layer planes, perpendicular to the extrusion/deformation direction. Normal direction (ND) patterns of the films were obtained by aligning the incident X-ray beam perpendicular to the plane of the film. The WAXS patterns were collected using a magnetic imaging plate, which is processed using a Fujifilm PLA700 image reader after 2 h of exposure in TD, and 17 h of exposure in ND. The sample-to-detector distance was 150 mm and the diffraction angle was calibrated using a CaF_2 standard.

Changes in crystallinity and crystal structure due to the stretching process were measured using differential scanning calorimetry (DSC). Two first heating thermograms were obtained for each film at each strain on a Perkin-Elmer Pyris 1 differential scanning calorimeter (DSC) at a heating rate of 40 °C min^{-1}, and normalized by sample weight. This fast heating rate was chosen to avoid recrystallization of the PEO during the heating process. Calculated average crystallinity values were obtained by deconvolution of these thermograms and were corrected for weight composition. This was done by conversion of volume composition to weight composition, using the density of EAA, 0.936 g/cm^3, and the density of the PEO amorphous fraction, 1.124 g/cm^3, as PEO is amorphous during the coextrusion process.[23]

RESULTS AND DISCUSSION

Tensile Testing of Multilayered Films. Stress–strain curves of EAA/PEO and control films are shown in Figure 1,

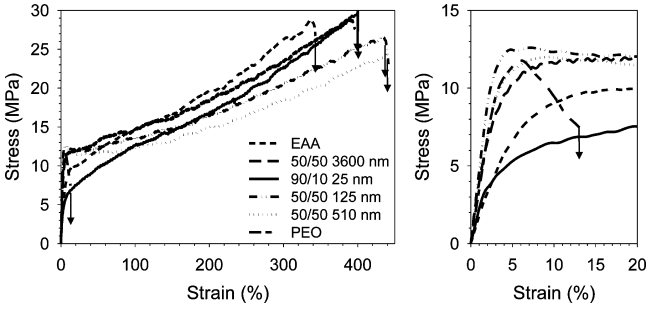

Figure 1. Representative stress–strain curves of EAA/PEO and controls (room temperature, 100%/min) showing (a) films retained ductility of EAA and (b) increase in the modulus and yield stress, and decrease in the yield strain with decreasing layer thickness.

Table 2. Layered Sample Characteristics

EAA/PEO (v/v)	number of layers	nominal EAA layer thickness (nm)	nominal PEO layer thickness (nm)	EAA X_c (by wt%)	PEO X_c (by wt%)
0/100	1025			0	93
50/50	33	3600	3600	21	74
50/50	257	510	510	20	82
50/50	1025	125	125	24	72
90/10	1025	220	25	31	92
100/0	1025			38	0

Table 3. Tensile Properties EAA/PEO (100%/min, T = 23°C, n = 3)

EAA/PEO (v/v)	no. layers	nominal layer thickness (nm)	1% composite modulus (MPa)	1% PEO modulus (MPa)	yield strain (%)	yield stress (MPa)	fracture strain (%)	fracture stress (MPa)
0/100	1025		428 ± 38	428 ± 38	5.0 ± 1.0	9.0 ± 0.3	14 ± 2	8 ± 1
50/50	33	3600	313 ± 67	486 ± 84	16.2 ± 1.9	12.0 ± 0.6	400 ± 31	29 ± 2
50/50	257	510	360 ± 25	579 ± 43	10.6 ± 1.3	11.3 ± 1.1	410 ± 41	23 ± 2
50/50	1025	125	413 ± 68	685 ± 85	6.4 ± 0.1	12.2 ± 0.5	410 ± 41	25 ± 2
90/10	1025	25	272 ± 67	1450 ± 99			400 ± 5	28 ± 1
100/0	1025		141 ± 37		18.0 ± 0.1	9.9 ± 0.1	340 ± 18	29 ± 1

and the measured tensile properties are summarized in Table 3. PEO controls were extremely brittle, fracturing at (14 ± 2)% strain. EAA control films exhibited ductile behavior, with gradual yielding, and fracturing at (340 ± 18)% strain. The multilayered films retained the ductility of EAA, unaffected by the 10% or 50% volume fraction of brittle PEO, or by the scale of the layers. All layered films exhibited similar fracture strains and stresses to the EAA control. As the composition of the layered films were not the same, the PEO modulus was calculated from the composite modulus, according to the parallel model, as was done previously:[19]

$$E_{PEO} = \frac{E_{composite} - E_{EAA}V_{f,EAA}}{V_{f,PEO}} \quad (1)$$

E_{PEO}, E_{EAA}, and $E_{composite}$, are the moduli of the PEO, the EAA, and the composite, respectively, and $V_{f,PEO}$ $V_{f,EAA}$, and $V_{f,composite}$ correspond to the volume fractions of the PEO, the EAA, and the composite, respectively.

The PEO modulus increased significantly as PEO layer thickness decreased. There appeared to be no significant effect of layer thickness on yield stress, but a decrease in the yield strain was observed, with no detectable yield point when PEO layer thickness approached the thickness of a single lamella. The reinforcement was due to stress redistribution to the higher modulus aligned PEO lamellae within the layers.[19] The lower yield strain observed was most likely due to a decrease in interlamellar fractions between PEO lamellae in the deformation direction as the PEO lamellae became more and more aligned in the deformation direction.

Stress-whitening was also observed in all films, regardless of layer thickness. The effect was much more pronounced in thicker layers than in thin layers. This was to be expected, as 125 and 25 nm layers are on the order of the quarter wavelength of visible light, which would give the films a more transparent appearance even before stretching down the layer thicknesses.[24] The morphology differences between the different layer thicknesses also greatly affect the stress-whitening. In thick layers that contain spherulites or truncated spherulites (3600 and 510 nm), there are large amounts of interlamellar amorphous fractions perpendicular to the deformation axis that will stretch and result in voids that scatter light.[1,25] Thin layers, however, have less interlamellar spaces due to greater orientation of the crystalline fraction, and the amorphous fraction is excluded into spaces that are also aligned with the deformation direction. After uniaxial stretching, each film was clamped at 0%, 50%, 100%, 150%, 250%, and 400% strains for 2D wide-angle X-ray diffraction to determine the large-scale orientation of the crystalline fraction at each point along the stress−strain curve.

Wide Angle X-ray Diffraction: Large-Scale Structural Analysis. 2D WAXD patterns with the X-ray beam parallel to the layer planes, perpendicular to the deformation/extrusion axis (transverse), and perpendicular to the plane of the film (normal), were collected for each sample. PEO, at 0% strain, and EAA controls, at 0% and 400% strain, are shown in Figure 2. The WAXD pattern of the monoclinic crystal form of PEO

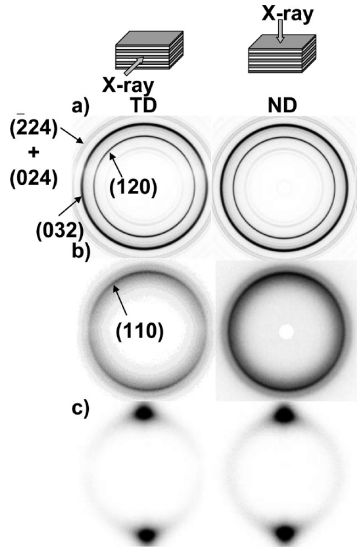

Figure 2. 2D WAXD patterns of control films: a) PEO in transverse and normal directions at 0% strain, EAA control in both transverse and normal directions at b) 0% strain and c) 400% strain. (PEO control fractured at ∼14% strain).

had a ring at scattering angle 2θ = 19.28°, corresponding to the reflections from (120) planes, and a second ring at 2θ = 23.38°, containing the overlapping reflections from the (032), ($\bar{1}$32), (112), ($\bar{2}$12), ($\bar{1}$24), ($\bar{2}$04), and (004) planes.[26,27] (120) and (032) reflections were observed as concentric rings in both transverse (TD) and normal directions (ND), indicating no particular orientation of the PEO crystals. Very weak ($\bar{2}$24) and (024) reflections (2θ = 26.38) were also present. These reflections were not used for analysis since the full spectrum of these reflections could not be obtained due to the distance between sample and detector, limiting interpretation of crystal orientation. With the X-ray beam perpendicular to the plane of the film (ND), all reflection planes produced concentric rings, indicating isotropic orientation. No patterns were collected at 400% strain for PEO, as PEO is very brittle, and fractured at ∼14%. As-extruded EAA control films showed similar patterns in both TD and ND. At 0% strain, EAA showed an isotropic ring of the orthorhombic (110) reflection from the PE comonomer.[28,29] When stretched to 400%, the EAA control displayed a concentrated, largely amorphous, spot on the meridian, indicating alignment of the chains along the deformation axis, in both TD and ND.

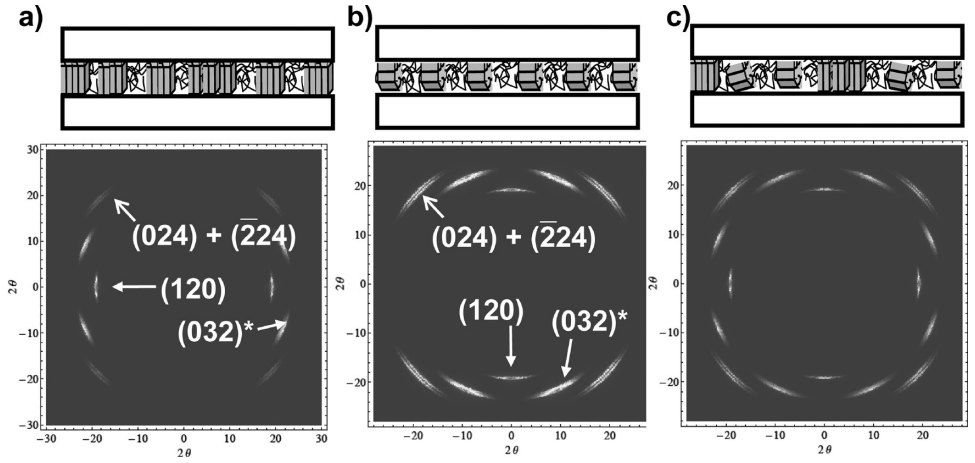

Figure 3. Simulated 2D WAXD patterns of the possible PEO structures in the transverse directions (TD): a) in-plane, b) edge-on, b) mixed in-plane and edge-on. *Arcs are a combination of overlapping reflections from (032), ($\bar{1}$32), (112), ($\bar{2}$12), ($\bar{1}$24), ($\bar{2}$04), and (004).

Layered samples stretched to 0%, 50%, 100%, 150%, 250%, and 400% strains were tested under the same conditions. Figure 3 displays simulated TD 2D WAXD patterns of the possible PEO crystal structures that can occur: in-plane, edge-on, and mixed in-plane and edge-on. In-plane orientation, where the chain orientation is perpendicular to the layer plane, is characterized by equatorial (120) arcs and (032) reflections at azimuthal ϕ = 67°, 113°, 237°, and 293° with respect to the meridian. ($\bar{2}$24) and (024) reflections (2θ = 26.38) will appear at azimuthal ϕ = 45° (Figure 3a). Edge-on lamellae with fiber orientation exhibits a similar pattern to the in-plane, only turned 90 degrees, with reflections aligned along the meridian (Figure 3b). A mixed in-plane and edge-on orientation results in superimposed patterns of the in-plane and edge-on orientation patterns (Figure 3c).

It was reported previously that the morphology of the EAA layers does not change with layer thickness.[18] As EAA is stretched as a control, as well as within the layered films, the isotropic (110) reflection and amorphous ring gradually concentrate along the meridian, indicating alignment of the EAA chains along the deformation axis. All layered film patterns indicated EAA qualitatively behaves in the same manner in all samples, regardless of layer thickness. Therefore, EAA layers were disregarded in the layered films, and we will only discuss structural changes of the PEO layer.

Thick Layers—Spherulitic Morphology. Above 510 nm PEO layers, 2D WAXD showed similar results at each strain. Figures 4 and 5 show 2D WAXD patterns of layered EAA/PEO with 3600 and 510 nm PEO layers, respectively, in both transverse and normal directions (TD and ND) at 0%, 150%, and 400% strains, with corresponding sketches of the PEO morphology confined within the layered structure. Thick layers show concentric rings at 0% strain, in both TD and ND, of the (120) and (032) reflections, indicating isotropic orientation of the PEO crystals. At 510 nm, there is an expected spatial limitation in the layer thickness direction on the spherulite, and is therefore sketched as a truncated spherulite.

When these films are stretched to 50% strain (data not shown), TD broad meridional (120) and (032) arcs appear, indicating the presence of loosely edge-on PEO crystals in all samples. As they are stretched to 100% strain (data not shown), these edge-on reflections grow stronger, while maintaining much of the original orientation. Due to the initial spatial constraint of the 510 nm PEO layers, these samples began to

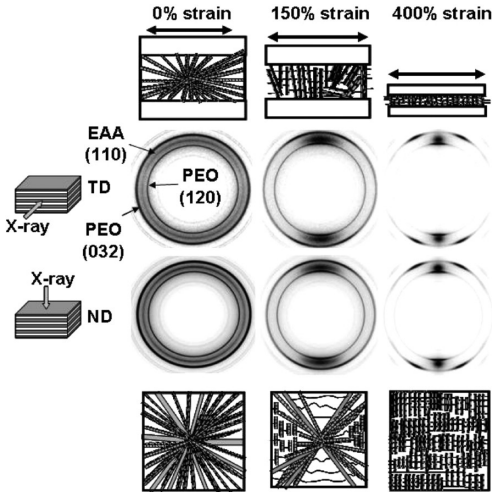

Figure 4. 2D WAXD patterns of 50/50 EAA/PEO 3600 nm in both transverse and normal directions (TD and ND) at 0%, 150%, and 400% strain, with sketches of the PEO layer structure.

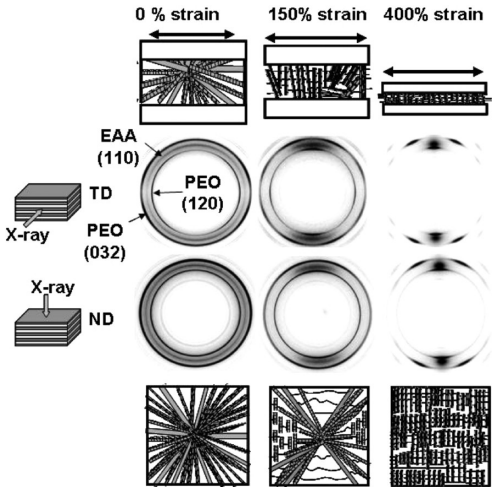

Figure 5. 2D WAXD patterns of 50/50 EAA/PEO 510 nm in both transverse and normal directions (TD and ND) at 0%, 150%, and 400% strain, with sketches of the PEO layer structure.

display smaller, more concentrated arcs along the equator as well. In the normal direction, corresponding meridional arcs appear, while maintaining a weak isotropic ring, indicating a gradual alignment of the crystals in the direction of deformation. At 150% strain, the edge-on crystal reflections become stronger as broken crystals are turned or chains are pulled out and recrystallized along the deformation axis. The TD edge-on reflections continued to grow stronger from 250% to 400% strain. At this point, all chains have become aligned with the deformation axis within 510 and 3600 nm layers, and resulted in similar patterns in both the TD and ND, analogous to a typical PEO fiber pattern.[30,31] Essentially, layers of 510 nm or thicker behave like bulk semicrystalline polymers.

Thin Layers–Aligned PEO Lamellae Morphology. Figure 6 and Figure 7 show 2D WAXD patterns of the layered

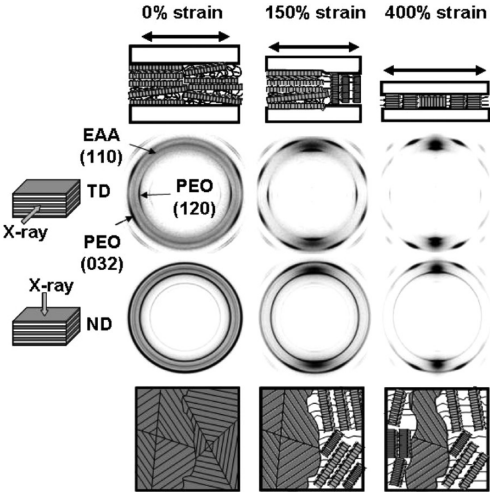

Figure 6. 2D WAXD patterns of 50/50 EAA/PEO 125 nm in both transverse and normal directions (TD and ND) at 0%, 150%, and 400% strain, with sketches of the PEO layer structure.

films with PEO layer thickness 125 and 25 nm, respectively, stretched to 0%, 150%, and 400% strain. Corresponding sketches of the PEO morphology confined within the layered structure are also shown. Unstretched 125 nm films showed

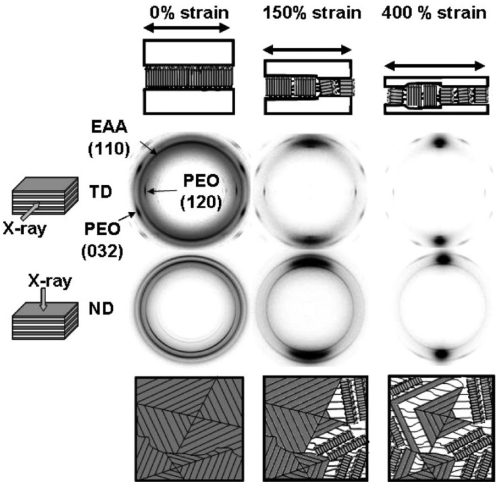

Figure 7. 2D WAXD patterns of 90/10 EAA/PEO 25 nm in both transverse and normal directions (TD and ND) at 0%, 150%, and 400% strain, with sketches of the PEO layer structure.

TD (120) reflections as wide arcs along the equator, representing loosely aligned PEO crystals, where not all lamellae are parallel to the layer plane. ND patterns still exhibited isotropic orientation, resulting in a sketch of loose stacks of PEO lamellae. When the layer thickness approached the thickness of a single PEO lamella, ~25 nm, 2D WAXD patterns showed concentrated (120) equatorial arcs in the TD, while maintaining isotropic orientation in the ND. It must be noted that in-plane crystals do not give strong reflections when the X-ray beam is parallel to the (120) face, and therefore, were difficult to detect in the ND.

As these thinner PEO layer films were stretched to 50%, 100%, and then 150% strain, the (120) equatorial arcs became smaller and more concentrated, much like the 510 nm layer films. This behavior was most likely due to forced alignment of the loosely in-plane crystals as the layers were thinned under strain. It is suggested that micronecking (nonuniform deformation) was present within thinner 125 and 25 nm layers, as the initial PEO structures were such that uniform thinning of the PEO layers would be difficult. Many single crystal studies of various semicrystalline polymers, such as PE and PP, have shown evidence of such nonuniform deformation at strains between 30 and 100% with fibrils connecting sections of undeformed crystal.[13,14] ND patterns showed a continuation of the gradual alignment of the chains in the direction of deformation, with strengthened meridional reflections. At 400%, however, these thin layers still retained some in-plane crystals, which resulted in incongruent TD and ND X-ray patterns, as in-plane (120) crystal faces are parallel to the ND X-ray beam and cannot be detected.

In order to compare the different samples at each strain more quantitatively, the peak intensities of PEO (120) in-plane and edge-on crystals were obtained from 2D WAXD integrated intensity scans. An example using 90/10 25 nm at 400% strain patterns in the transverse and normal directions is shown in Figure 8a and b, respectively. The intensity of the (120) reflection in each direction was obtained by subtracting the baseline to give $I_{120,\ \text{on-edge}}$ (along the meridian) and

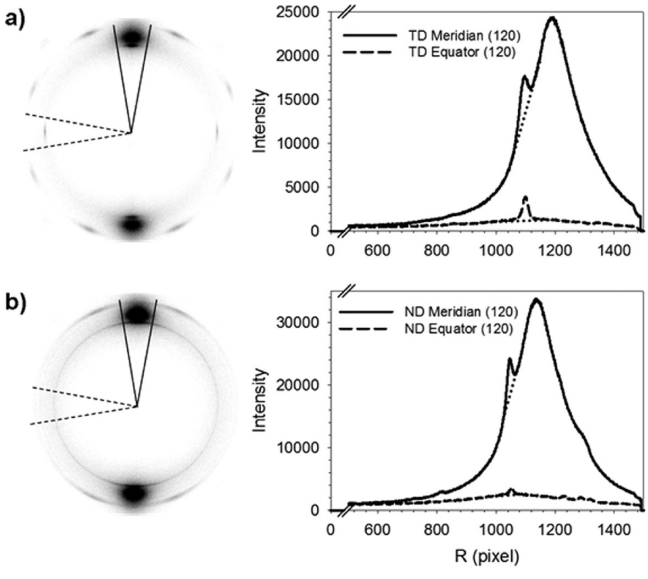

Figure 8. (a, b) Obtaining the peak intensities of PEO (120) in-plane and edge-on crystals from 2D WAXD integrated intensity scans, 90/10 25 nm, 400% strain: (a) transverse direction and (b) normal direction.

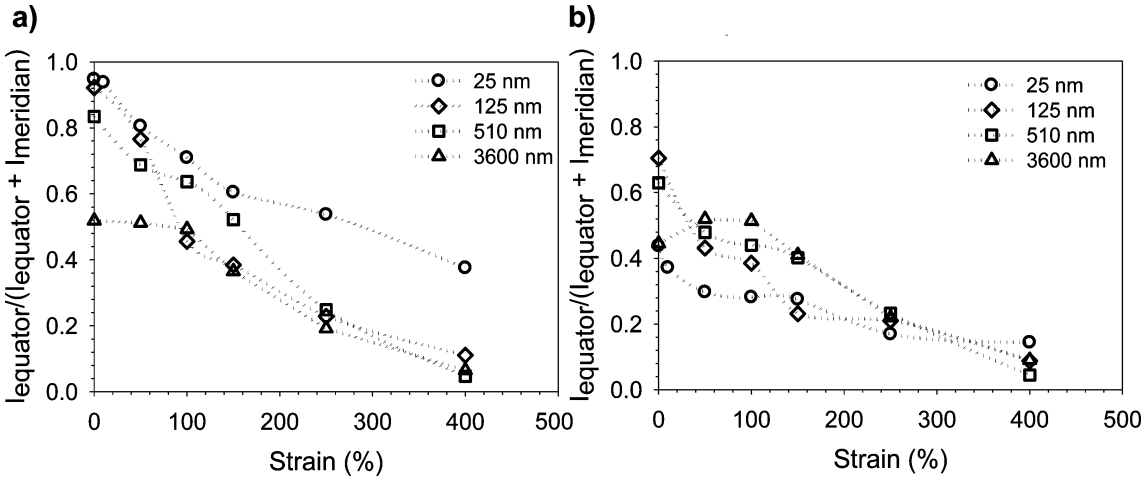

Figure 9. (a, b) Transition of PEO (120) crystal face orientation with uniaxial strain in the (a) transverse direction and (b) normal direction.

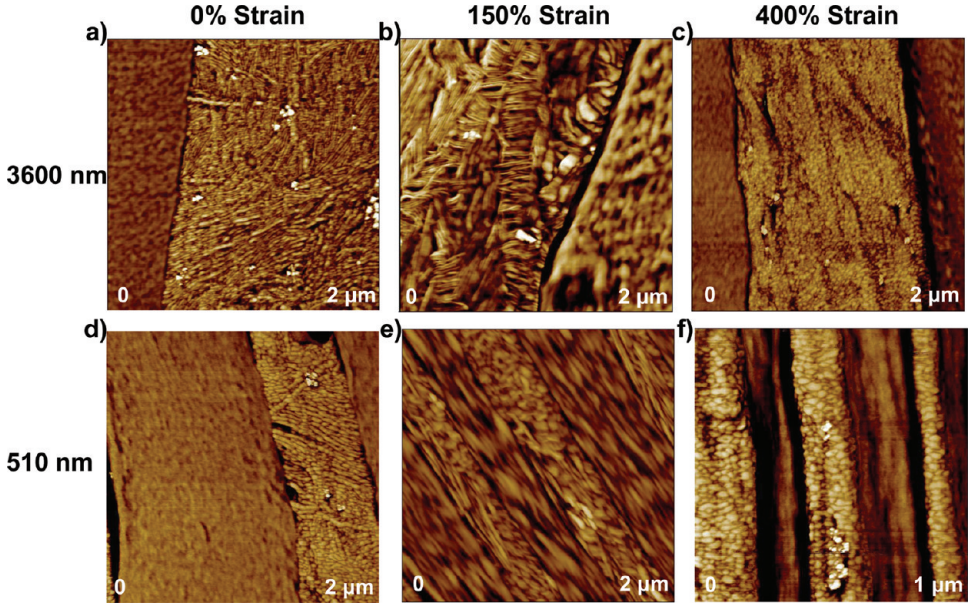

Figure 10. (a–f) Comparisons of thick PEO layer EAA/PEO AFM images: Vertical = PEO layer thickness effect; horizontal = effect of strain.

$I_{120,\ in\text{-}plane}$ (along the equator). Percentages of crystals with in-plane orientation were compared for different strains, rather than absolute values, by dividing the equatorial (120) peak intensity by the total (Figure 8a and b). This was done so that comparisons could be made between the different layer thicknesses and strains, which varied in overall thickness and composition.

Figure 9a and b shows the change in fraction of in-plane crystals with strain in the transverse and normal directions, respectively. As the layer thickness decreases, the amount of initial in-plane orientation increases, reaching 100% at the 25 nm layer thickness. As the samples are stretched, the in-plane crystal fraction within thicker layers of 125 nm and greater, gradually decrease to 15% or less once at 400% strain. In contrast, the in-plane crystal fraction in 25 nm PEO layers decreased at a slower rate, and about 40% of the original in-plane orientation remains even at 400% strain. Normal direction intensities begin around 50%, which was expected, as all samples exhibited isotropic 2D WAXD patterns in this direction. All layer thicknesses showed similar decreases with strain, due to the inability to detect in-plane (120) reflections in this direction. The large amount of in-plane crystals retained in these samples could be due to simple spatial confinement and mechanical reinforcement of the crystals. Another possibility is that, like polyester and polyethylene single crystals, the direction of deformation along the crystal growth planes can result in different tilt processes that may leave crystals aligned toward one direction undeformed.[12,14] Since the PEO is randomly aligned in the plane of the film, it is highly likely that roughly half of the crystals were oriented at an angle that did not allow deformation, resulting in the retention of roughly half the original in-plane crystals.

Atomic Force Microscopy: Small Scale Structural Analysis. Atomic force microscopy (AFM) images were taken of EAA/PEO film cross sections at 0%, 150%, and 400% strain to observe the small scale morphological changes that occurred under deformation. The images collected were then compared to the predicted PEO structures from WAXD patterns at each strain point sampled, Figures 10a–f and 11a–f. The EAA possesses low crystallinity and a lower modulus than PEO, and appeared as a smooth, dark phase. PEO, with its high

dx.doi.org/10.1021/am300240r | ACS Appl. Mater. Interfaces 2012, 4, 2218–2227

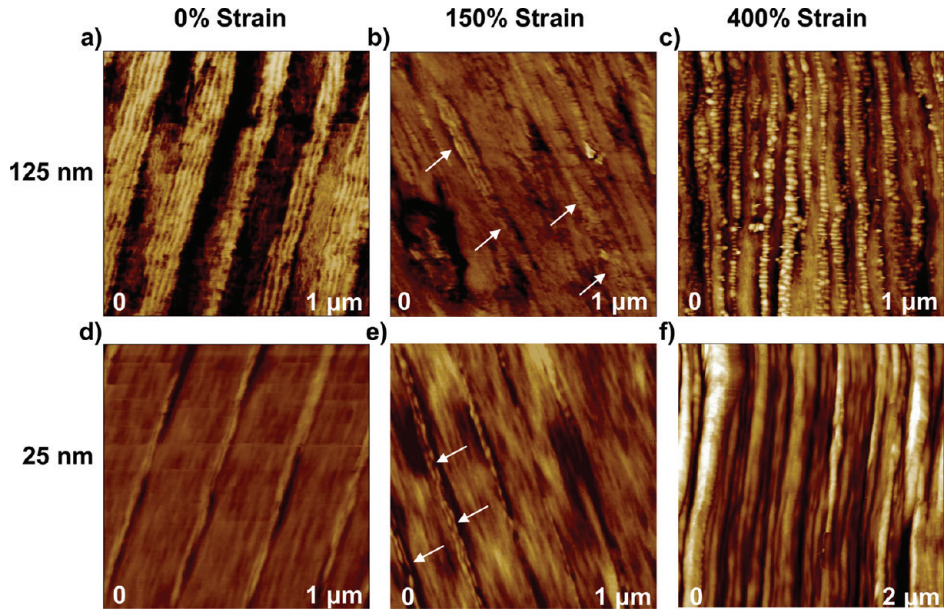

Figure 11. (a–f) Comparisons of thin PEO layer EAA/PEO AFM images: Vertical = PEO layer thickness effect; horizontal = effect of strain. Arrows point to signs of nonuniform deformation.

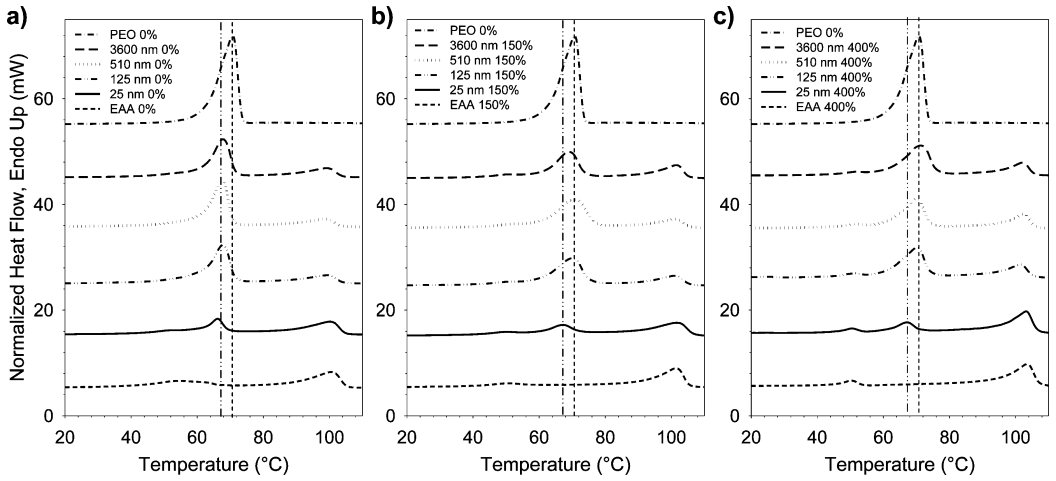

Figure 12. (a–c) Heating differential scanning calorimetry thermograms of EAA/PEO at (a) 0% strain, (b) 150% strain, and (c) 400% strain. Vertical lines are to guide the eye. Dashed lines are drawn at 71 °C. Dash-dot-dot lines are drawn at 68 °C. PEO control at 0% strain has been plotted in each graph for comparison as well.

crystallinity, and higher modulus, appeared as the light phase, with apparent crystalline structures.

Thick Layers–Spherulitic Morphology. Unstretched thicker PEO layers showed spherulitic features that deformed similar to bulk semicrystalline polymers. 50/50 3600 nm PEO layers contained large spherulites, 1–2 of which spanned the width of the layer (Figure 10a). 50/50 510 nm PEO layers showed truncated spherulites that spanned the full width of the layer with no preferential orientation of the crystals (Figure 10d). These images are in good agreement with the AFM images obtained in an earlier study published by Wang et al.[18]

When stretched to 150% strain, both 3600 and 510 nm PEO layers displayed a mixture of stacked in-plane lamellae and broken edge-on crystals in layers of uniform thickness (Figure 10b and e). Stretching to 400% strain resulted in multiple edge-on crystallites spanning the layer thickness, most likely arising from recrystallization (Figure 10c and f).

Thin Layers–Aligned PEO Lamellae Morphology. One hundred twenty-five nanometer layers were composed of aligned lamellar stacks, 5–6 lamellae thick. These stacks were primarily aligned parallel to the layer plane, with some tilting (Figure 11a). Twenty-five nm layers showed single PEO lamellae confined between the EAA layers (Figure 11d). These images are in good agreement with the AFM images obtained in an earlier study.[18] Micronecking was indeed present in 125 nm layers, as thinned areas made up of most likely recrystallized edge-on PEO crystallites and nondeformed sections of aligned stacked lamellae were observed (Figure 11b). As the 25 nm PEO layers are stretched to 150%, small gaps are observed between the single lamellae, which could either be cracks in broken crystals, or widening gaps between undeformed crystals. A bead-like structure was also observed (Figure 11e). This structure may arise from the nonuniform thinning of the lamellae, as they undergo chain tilting and chain slip with deformation. At 400% strain, 125 nm layers were composed of

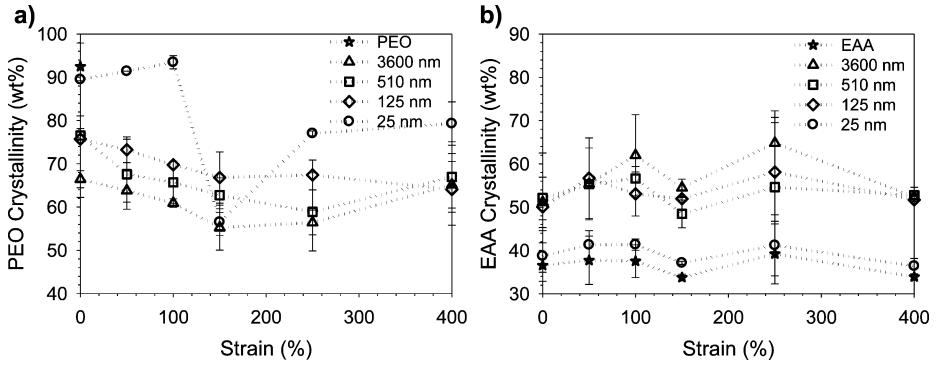

Figure 13. (a, b) Calculated crystallinity (by weight) from DSC thermograms (corrected from weight composition): (a) PEO and (b) EAA.

single edge-on crystallites spanning the layer thickness, as these layers have become very thin with strain (~25 nm) (Figure 11c). The thin, single lamella thickness layers were obscured by recovered EAA at high strain, and the PEO layers could not be visualized. (Figure 11f). In general, as the layer thickness decreases, thick PEO layers undergo axial alignment of the crystalline fraction, as seen in bulk materials, while thinner layers (<125 nm) deform nonuniformly through micronecking, similar to findings of solution-grown single and multilayer crystals literature.

Thermal Behavior. Differential scanning calorimetry was performed on layered EAA/PEO films to give insight into the structure and stability of the crystals. The raw first heating endotherms for samples stretched to 0%, 150%, and 400% strains are shown in Figure 12a–c. PEO control films exhibit a sharp melting endotherm at 71 °C, consistent with aged PEO.[32] EAA control films display a polyethylene (PE) melting endotherm at 98 °C and a smaller melting peak of secondary crystallites at 50 °C, related to unstable PE crystals due to hydrogen bonding of the carboxylic acid groups.[28,33] Thicker unstretched films with 3600, 510, and 125 nm PEO layers showed EAA melting peaks at the same temperatures as the controls, but a lowered PEO melting peak at 68 °C. The 90/10 composition film exhibited the same behavior for EAA as the control, but PEO melting was depressed further than in the other layered films, 66 °C. This behavior may be due to less perfect PEO crystals, as pure PEO single crystal fragments are often formed at different sites and connected by loosely packed crystals and tie chains, especially in the case of high molecular weight, resulting in lower packing energy, and a lower melting temperature.[34] All PEO melting temperatures were elevated from the previously published value of 65 °C,[17,18] however, due to aging of the PEO. Exposure to water in the atmosphere before drying plasticized the PEO, and allowed for better packing and further crystallization.[32]

Stretching to 150% strain resulted in the broadening of the PEO peaks as the PEO strain-recrystallized, producing crystallites that melt at higher temperature, ~71 °C for thicker layers and ~68 °C for 25 nm PEO layers. It should be noted here that the PEO control at 0% strain is plotted in each graph at each strain, as PEO fractured at 14% strain, to help emphasize the temperature shifts of the layered PEO melting peaks. At 400%, the strain-recrystallized PEO melting peak strengthened and the original PEO crystallites decreased, sharpening the broadened peak from 150% strain toward the higher melting temperatures. A shift of the melting peaks of EAA to 52 and 100 °C was also observed, indicating strain-induced recrystallization was present in the EAA layers as well. All thicker PEO layer films appeared almost identical, as was observed with TD WAXD. The 25 nm PEO layer film is visibly different, with slightly downshifted melting peaks (2 °C), and a slightly smaller peak shift with strain.

The weight percent crystallinity of the PEO and EAA fractions were calculated from ΔH_m of each heating thermogram, using heat of fusion values of 197 J/g for PEO crystals[35] and 290 J/g for PE crystals,[36] correcting for weight composition of each sample. PEO control was determined to be 90% crystalline, significantly higher than previously reported,[17−19] due to water absorption and redrying[32] (Supporting Information Figure 1). PEO crystallinity within layers was lower, however, ranging between 66 and 80%, with thicker layers of 125 to 3600 nm possessing lower crystallinity values than the 25 nm single lamellae layers. EAA control was determined to be 37% crystalline, consistent with previously reported values.[18] Films with 90/10 vol/vol composition EAA/PEO possessed similar EAA crystallinity to the control, 35%, but those with a 50/50 vol/vol composition possessed elevated EAA crystallinity, ranging from 45 to 52%. It is possible that the aging of the PEO nucleated further crystallization of the EAA within these films, and the effect is more apparent in the EAA/PEO 50/50 compositions, as these EAA layers are thinner compared to the 90/10 composition and EAA control.

As these films were stretched, the PEO crystallinity was expected to decrease as crystals were broken up and chains pulled out from the lamellae, followed by an increase as the chains underwent strain-induced recrystallization, with a possible subsequent decrease as a result of further orientation and fracture of the newly crystallized structures as it neared fracture of the sample.[1−8,25] However, only the thicker PEO layers exhibited this progression, while the thinnest layers exhibited an initial increase in crystallinity before decreasing and increasing once again, Figure 13a. The crystallinity of the thickest PEO 3600 nm layers decreases gradually to 250% due to its isotropic orientation. The amount of interlamellar deformation before breakage and unfolding of crystals was greatest in these layers, since a large amount of PEO lamellae were aligned perpendicular to the deformation axis. Films with PEO layer thicknesses of 510 nm exhibited very similar behavior to the 3600 nm, as suggested by 2D WAXD. The crystallinity of the 125 nm PEO layer also gradually decreases, but at a slower rate than the thicker layers, most likely due to the reinforcement resulting from the highly aligned PEO lamellar stack morphology.

Further reduction of the PEO layer thickness to 25 nm, with a single lamella aligned in the deformation direction, resulted in the initialization of chain pullout and strain recrystallization at

an earlier strain point, ≤50%, than observed in thicker PEO layers. This was exhibited as a small initial increase in the crystallinity before the expected decrease and subsequent increase. It was previously discovered that these thinner layers were significantly mechanically reinforced due to the crystal orientation,[19] which would require larger stresses to bring about lamellar tilting, breakage, and unfolding. Therefore, the small amount of strain recrystallization initially found in these layers most likely originated from crystalline defects and lamellar edges. Enhanced reinforcement of the 25 nm layers caused a delay in the full onset of strain recrystallization to between 150 and 250% strain.

Though strain-induced recrystallization was observed in the EAA layers, the change in EAA crystallinity with stretching did not vary significantly with layer thickness. Crystallinity values of films with 50/50 composition were comparable at each strain point, even possessing the same amount of EAA crystallinity, 52%, near the film fracture point. The 90/10 composition film and EAA control film behaved analogously, with lower crystallinity than the 50/50 composition films. These results support the earlier assumption that EAA deformation is not affected by the layer thickness.

CONCLUSIONS

The effect of confinement on the deformation behavior of poly(ethylene oxide) was studied using melt processed coextruded EAA and PEO multilayer films with varying PEO layer thicknesses from 3600 nm down to 20 nm. The deformation mechanism was found to shift as layer thickness was decreased between 510 and 125 nm. This change was evaluated with tensile testing, wide-angle X-ray diffraction (WAXD), atomic force microscopy (AFM), and differential scanning calorimetry (DSC).

In general, layers of 510 nm or thicker behaved like bulk semicrystalline polymers. The spherulitic structure within these layers underwent interlamellar and intralamellar deformation through the yield point, followed by subsequent chain pull-out and recrystallization. These samples showed a gradual progression from isotropic orientation of the PEO crystals to almost full (>85%) orientation of the chains along the deformation axis with concentrated meridional (120) arcs, like that of a typical PEO fiber.

Films with 125 and 25 nm exhibited similar features to those observed in the literature of single crystals and single crystal mats.[9−14,19] As these films were stretched, the lamellae became increasingly aligned with the deformation direction, cracking, and micronecking as strain increased. Single crystal thicknesses underwent strain-induced recrystallization, while retaining ∼40% of is original in-plane orientation, unlike any of the other layer thicknesses. The large amount of in-plane crystals retained in these samples could be due to simple spatial confinement and mechanical reinforcement of the crystals. Another possibility is that, like polyester and polyethylene single crystals, the direction of deformation along the crystal growth planes can result in different tilt processes; micronecking and uniform deformation takes place when stretched along one axis, with minimal deformation and cracking when stretched along the other axis.

In general, as the layer thickness decreases, thick PEO layers undergo axial alignment of the crystalline fraction, as seen in bulk materials, while thinner layers (≤125 nm) deform nonuniformly through micronecking, as literature of solution-grown single and multilayer crystals has previously discussed. With the commercially relevant method of melt coextrusion, we overcame the limitations associated with the testing of solution-grown single crystals, and the artifacts that occur from their handling, and bridged the gap in knowledge between thick bulk materials and thin single crystals. The discovery of this shift in deformation mechanism that occurs between 510 and 125 nm due to crystal orientation can be very useful for future design of materials incorporating semicrystalline polymers in confined spaces where mechanical properties are integral.

ASSOCIATED CONTENT

Supporting Information

To verify the effect of water and aging on the melting of PEO, the same sample was subjected to cycles of melting and water absorption, and the melting peak position and crystallinity were examined. The results confirmed that the PEO does indeed age with water absorption, resulting in elevated melting peak, and increased crystallinity. This information is available free of charge via the Internet at http://pubs.acs.org/.

AUTHOR INFORMATION

Corresponding Author

*Phone: (216) 368-1421. E-mail: lashanda.korley@case.edu.

Notes

The authors declare no competing financial interest.

†Deceased on 9/6/2010

ACKNOWLEDGMENTS

This project was made possible through the generous financial support of the National Science Foundation Science and Technology Center, Center for Layered Polymeric Systems (DMR-0423914).

REFERENCES

(1) Adams, W. W.; Yang, D.; Thomas, E. L. *J. Mater. Sci.* **1986**, *21*, 2239−2253.
(2) Saraf, R. F.; Porter, R. S. *J. Polym. Sci. Polym. Phys.* **1988**, *26*, 1049−1057.
(3) Lin, L.; Argon, A. S. *J. Mater. Sci.* **1994**, *29*, 294−323.
(4) Li, J. X.; Cheung, W. L.; Chan, C. M. *Polymer* **1999**, *40*, 3641−3656.
(5) Men, Y. F.; Rieger, J.; Strobl, G. *Phys. Rev. Lett.* **2003**, 91.
(6) Geil, P. H.; Ginzburg, B. M. *J. Macromol. Sci. B* **2006**, *45*, 291−323.
(7) Seguela, R., *e-Polymers*; 2007.
(8) Bartczak, Z.; Galeski, A. *Macromol. Symp.* **2010**, *294-I*, 67−90.
(9) Garber, C. A.; Geil, P. H., *Makromol. Chem.* **1968**, *113*, 251-&.
(10) Gohil, R. M.; Patel, K. C.; Patel, R. D. *Colloid Polym. Sci.* **1974**, *252*, 358−366.
(11) Geil, P. H. *J. Polym. Sci., Part A* **1964**, *2*, 3813−3833.
(12) Kiho, H.; Peterlin, A.; Geil, P. H. *J. Polym. Sci. Polym. Lett.* **1965**, *3*, 257.
(13) Petermann, J.; Ebener, H. *J. Macromol. Sci. Phys.* **1999**, *B38*, 837−846.
(14) Shrawagi, S. R.; Thomas, E. L. *J. Polym. Sci. Pol. Phys.* **1976**, *14*, 799−809.
(15) Liu, R. Y. F.; Jin, Y.; Hiltner, A.; Baer, E. *Macromol. Rapid Commun.* **2003**, *24*, 943−948.
(16) Liu, R. Y. F.; Bernal-Lara, T. E.; Hiltner, A.; Baer, E. *Macromolecules* **2005**, *38*, 4819−4827.
(17) Wang, H. P.; Keum, J. K.; Hiltner, A.; Baer, E. *Macromolecules* **2009**, *42*, 7055−7066.
(18) Wang, H. P.; Keum, J. K.; Hiltner, A.; Baer, E.; Freeman, B.; Rozanski, A.; Galeski, A. *Science* **2009**, *323*, 757−760.

(19) Lai, C.; Ayyer, R.; Hiltner, A.; Baer, E. *Polymer* **2010**, *51*, 1820−1829.
(20) Mueller, C. D.; Nazarenko, S.; Ebeling, T.; Schuman, T. L.; Hiltner, A.; Baer, E. *Polym. Eng. Sci.* **1997**, *37*, 355−362.
(21) Ponting, M.; Hiltner, A.; Baer, E. *Macromol. Symp.* **2010**, *294-I*, 19−32.
(22) *ASTM Standard D1708: Standard Test Method for Tensile Properties of Plastics by Use of Microtensile Specimens*; ASTM International: West Conshohocken, PA, 2006.
(23) Huang, P.; Zheng, J. X.; Leng, S. W.; Van Horn, R. M.; Jeong, K. U.; Guo, Y.; Quirk, R. P.; Cheng, S. Z. D.; Lotz, B.; Thomas, E. L.; Hsiao, B. S. *Macromolecules* **2007**, *40*, 526−534.
(24) Jin, Y.; Tai, H.; Hiltner, A.; Baer, E.; Shirk, J. S. *J. Appl. Polym. Sci.* **2007**, *103*, 1834−1841.
(25) Pawlak, A. *Polymer* **2007**, *48*, 1397−1409.
(26) Tadokoro, H.; Chatani, Y.; Yoshihara, T.; Tahara, S.; Murahashi, S. *Makromol. Chem.* **1964**, *73*, 109.
(27) Wang, H. P.; Keum, J. K.; Hiltner, A.; Baer, E. *Macromol. Rapid Commun.* **2010**, *31*, 356−361.
(28) Baughman, T. W.; Chan, C. D.; Winey, K. I.; Wagener, K. B. *Macromolecules* **2007**, *40*, 6564−6571.
(29) Nakayama, K.; Kanetsuna, H. *J. Mater. Sci.* **1975**, *10*, 1105−1118.
(30) Takahashi, Y.; Tadokoro, H. *Macromolecules* **1973**, *6*, 672−675.
(31) Deitzel, J. M.; Kleinmeyer, J. D.; Hirvonen, J. K.; Tan, N. C. B. *Polymer* **2001**, *42*, 8163−8170.
(32) Kiss, D.; Suvegh, K.; Marek, T.; Devenyi, L.; Novak, C.; Zelko, R. *AAPS PharmSciTech* **2006**, 7.
(33) Kang, N.; Xu, Y. Z.; Wu, J. G.; Feng, W.; Weng, S. F.; Xu, D. F. *Phys. Chem. Chem. Phys.* **2000**, *2*, 3627−3630.
(34) Gu, F. M.; Bu, H. S.; Zhang, Z. *Polymer* **2000**, *41*, 7605−7609.
(35) Campbell, C.; Viras, K.; Richardson, M. J.; Masters, A. J.; Booth, C. *Makromol. Chem.* **1993**, *194*, 799−816.
(36) Wunderlich, B. *Macromolecular Physics*; Academic Press: New York, 1980; Vol. 3.